Mineralogy and Geochemistry of Host Rocks and Orebodies at the Anjing Hitam Prospect (Dairi, North Sumatra, Indonesia) and Their Environmental Implications

Rivai, Alvin Tomy
Department of Earth Resources Engineering, Graduate School of Engineering, Kyushu University

Yonezu, Kotaro
Department of Earth Resources Engineering, Graduate School of Engineering, Kyushu University

Syafrizal
Earth Resources Exploration Research Group, Faculty of Mining and Petroleum Engineering, Bandung Institute of Technology

Watanabe, Koichiro
Department of Earth Resources Engineering, Graduate School of Engineering, Kyushu University

https://doi.org/10.5109/2320997

出版情報：Evergreen. 6 (1), pp.18-28, 2019-03. 九州大学グリーンアジア国際リーダー教育センター
バージョン：

Mineralogy and Geochemistry of Host Rocks and Orebodies at the Anjing Hitam Prospect (Dairi, North Sumatra, Indonesia) and Their Environmental Implications

Tomy Alvin Rivai[1,*], Kotaro Yonezu[1], Syafrizal[2], Koichiro Watanabe[1]

[1]Department of Earth Resources Engineering, Graduate School of Engineering, Kyushu University, Japan

[2]Earth Resources Exploration Research Group, Faculty of Mining and Petroleum Engineering, Bandung Institute of Technology, Indonesia

*Author to whom correspondence should be addressed,
E-mail: tomyalvinrivai@mine.kyushu-u.ac.jp

(Received January 17, 2019; accepted March 22, 2019).

The Anjing Hitam prospect hosts Zn-Pb orebodies that may trigger environmental issues during its future mining and smelting activities. Therefore, the understanding of mineralogical and geochemical characteristics of host rocks and orebodies in this prospect is important to reveal. Concentration of sulfur in the host rocks is controlled by pyrite. Pyrite and sphalerite control concentration of sulfur in pyrite-rich massive ore while sphalerite and galena control concentration of sulfur in sphalerite-rich massive ore. Concentrations of cadmium and arsenic are strongly controlled by sphalerite and galena, respectively. Future mining and smelting activities at the Anjing Hitam prospect may give rise to several environmental issues, such as acid mine drainage, soil acidification and degradation, trace element contamination and human health problems.

Keywords: Mineralogy, geochemistry, host rocks, orebodies.

1. Introduction

The Dairi Zn-Pb deposit is located 290 km to the southwest of Medan city and 65 km to the northwest of the northern tip of Lake Toba, North Sumatra, Indonesia. Zn-Pb mineralization in the Dairi district is outlined at five prospects: Anjing Hitam, Lae Jehe, Basecamp, Bongkaras and Basuki Lode (Fig. 1a). Zn-Pb resources have been modeled for the Anjing Hitam, Lae Jehe and Basecamp prospects. At the Anjing Hitam prospect, total mineral resource is 8.1 million tons at 14.6% Zn and 9.1% Pb. The Lae Jehe and Basecamp prospects contain 16.2 million tons (8.2% Zn; 4.5% Pb) and 0.8 million tons (5.0% Zn; 5.0% Pb) ore, respectively. In terms of the current geological understanding of the Dairi Zn-Pb deposit, 69% of ore tonnage at the Anjing Hitam prospect is classified as measured resource, 27% as indicated resource and 4% of ore tonnage is inferred resource. At the Lae Jehe prospect, indicated and inferred resources constitute 50% ore tonnage for each while 100% ore tonnage at the Basecamp prospect is categorized as inferred resource (DPM, unpub., 2014). According to this data, the Anjing Hitam prospect is likely to be developed as the first mining site in the Dairi deposit.

Mining activities include rock excavation and its transportation as well as ore, waste and tailing dumping. An apparent impact of these activities is exposing buried rocks to the surface environments. Due to change of environments, the exposed rocks may become the sources of environmental issues. For instance, sulfide-rich rocks in surficial environments turn to be reactive and generate acid mine drainage (AMD) as they encounter runoff and rainwater. This behavior is contrast to sulfide-rich rocks below groundwater table where oxygen availability is limited (Aykol et al., 2003). During rock transportation, fine particles of excavated materials can be dispersed to atmosphere and decrease air quality around mine site[1)]. Dumping of ore, waste, and tailing can also significantly contribute to environmental issues associated with mining. High metal and sulfide concentration in ore and waste could be the main sources of acidity and metal contamination in water body and adjacent soils[1,2,3)]. In addition, although these pollutants are discharged to the environments during mining stage, their effects could extend for centuries post-mine closure[4,5,6,7)].

Since Cu, Zn, and Pb are considered to be the greatest causes of mining-related environmental issues among major metals (Fe, Al, Cu, Pb, Mn, Zn)[3)], base metal mining around the globe is regarded as a prominent contributor of pollutants[8,9,10,11,12,13)]. At the Anjing Hitam prospect, target metals are Zn and Pb. Future mining of Zn-Pb ore may produce other elements in the process, such as Cu, As and Cd. Accordingly, potential environmental issues may arise due to components of Cu,

Zn, Pb, Cd, As and S during and post mine development.

Through this study, we therefore aim to reveal mineralogical and geochemical characteristics of host rocks and orebodies at the Anjing Hitam prospect that potentially lead to environmental issues. The identification of potential environmental issues is essential to be carried out since pre-mining stage to ensure that future mining operation at the Anjing Hitam prospect complies with environmental regulations decreed by the Indonesian government[14]. Within this paper, we present our investigation results on macroscopic and microscopic characteristics of the host rocks and orebodies which exist in the Anjing Hitam prospect. We also supply concentrations of several key elements from the host rocks and orebodies. Subsequently, we interpret the data in terms of minerals controlling the element concentrations and their potential impacts to environment.

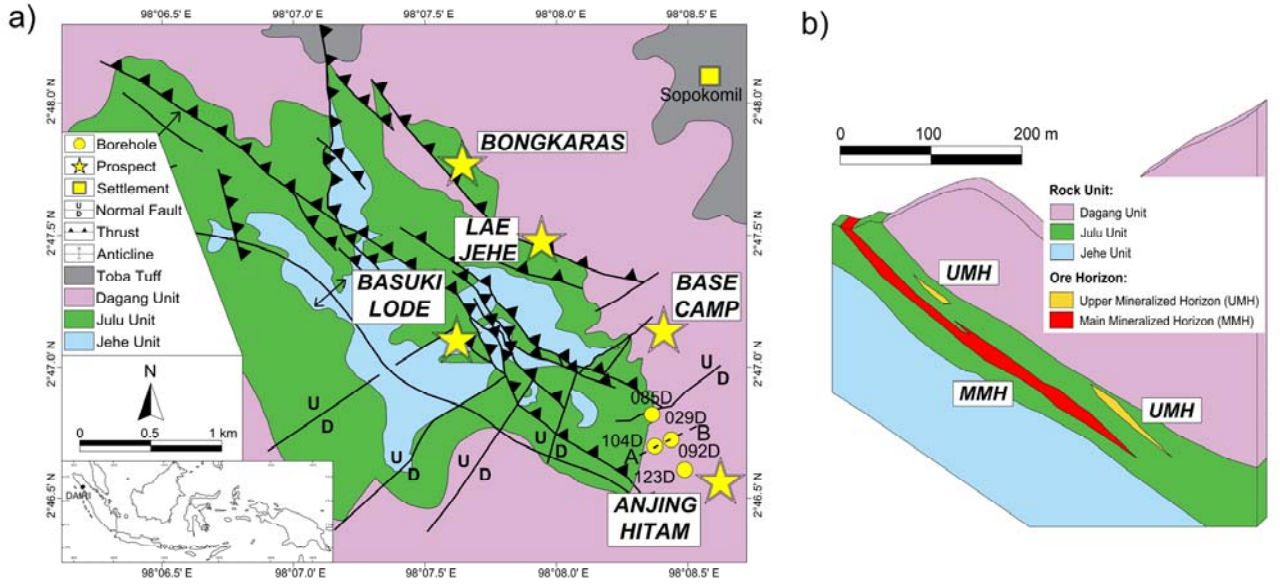

Fig. 1: (a) Geologic map of the Dairi deposit and (b) a cross section at the Anjing Hitam prospect. The cross section depicts subsurface geological condition along line A-B in Figure 1a. An index map in Figure 1a shows location of the Dairi deposit in Indonesia. Abbreviations: upper mineralized horizon (UMH), main mineralized horizon (MMH).

2. Geologic Background

Zinc-Pb orebodies in the Dairi deposit are distributed along a 4-km SE-NW strike in the eastern flank of the Sopokomil Dome. From top downward, the rocks in the Sopokomil Dome consists of interbedded calcareous siltstones-sandstones (Dagang unit), interbedded carbonaceous shales-calcareous siltstones (Julu unit) and massive as well as brecciated dolostones (Jehe unit)[15,16]. The Anjing Hitam prospect is situated in the southeastern portion of the Dairi deposit (Fig. 1a).

At the Anjing Hitam prospect, orebodies are hosted in the Julu unit and display stratiform and concordant morphologies[15]. Two mineralized horizons are present, namely the upper and main mineralized horizons. The upper mineralized horizon occurs as lenses and it is sporadically distributed throughout the prospect while the main mineralized horizon is continuous. The orebodies attain maximum thickness of 30 m in the main mineralized horizon (Fig. 1b).

3. Materials and Methods

Sixty-seven samples were selected from five boreholes in Anjing Hitam prospect (Fig. 1a). The selected boreholes represent southeastern (123D), central (092D, 104D, 029D) and northwestern (085D) portions of the prospect since the orebody is striking in the SE-NW direction. The boreholes in the central portion were chosen to represent the up-dip (104D), central (092D) and the down-dip (029D) portions as the orebody inclines to northeast. Of all the samples, only 22 represent the orebody and the rest are from host rocks within footwall and hanging wall sequences.

Doubly polished thin sections of representative host rock samples with thickness of approximately 0.03 mm were prepared to identify rock-forming minerals and their textural relationship. Likewise, thick polished sections were used to describe ore minerals and their relative abundance. Transparent and translucent minerals were observed by transmitted light while opaque and translucent minerals by reflected light. Petrography of host rocks and ore was carried out using a polarizing microscope NIKON ECLIPSE E600POL in Laboratory of Economic Geology, Kyushu University.

Concentrations of Zn, Pb, Cu, Cd, As and S of these samples were determined by a XRF Rigaku RIX300. Sample comminution was done using an iron mortar and

rod mills. The resulting powders were compacted at a pressure of 20 MPa for approximately 2 minutes in order to create XRF pellets. Pellet preparation and analysis were conducted in Laboratory of Economic Geology, Kyushu University.

4. Results

4.1 Host Rocks

The Dagang and Julu units are composed of quartz, carbonate minerals, muscovite and organic matter. Quartz and carbonate minerals are dominant in the sandstones and siltstones layers of the Dagang and Julu units while muscovite and organic matter are dominant in the shales layers of the Julu unit (Fig. 2a and b). Zircon and sphalerite occur in trace amounts in the Dagang and Julu units. Trace amounts of coarse-grained pyrite up to 500 µm in size are present in the Dagang unit while minor amounts of fine-grained pyrite less than 5 µm in size occur in the Julu unit. Although size of pyrite in the Julu unit is very fine, the Julu unit contains coarse-grained pyrite up to 3 mm in size hosted in quartz-carbonate veins parallel to the sediment laminations in the footwall sequence of the orebodies. In addition, these veins also host minor amounts of sphalerite, galena and occasionally chalcopyrite and pyrrhotite.

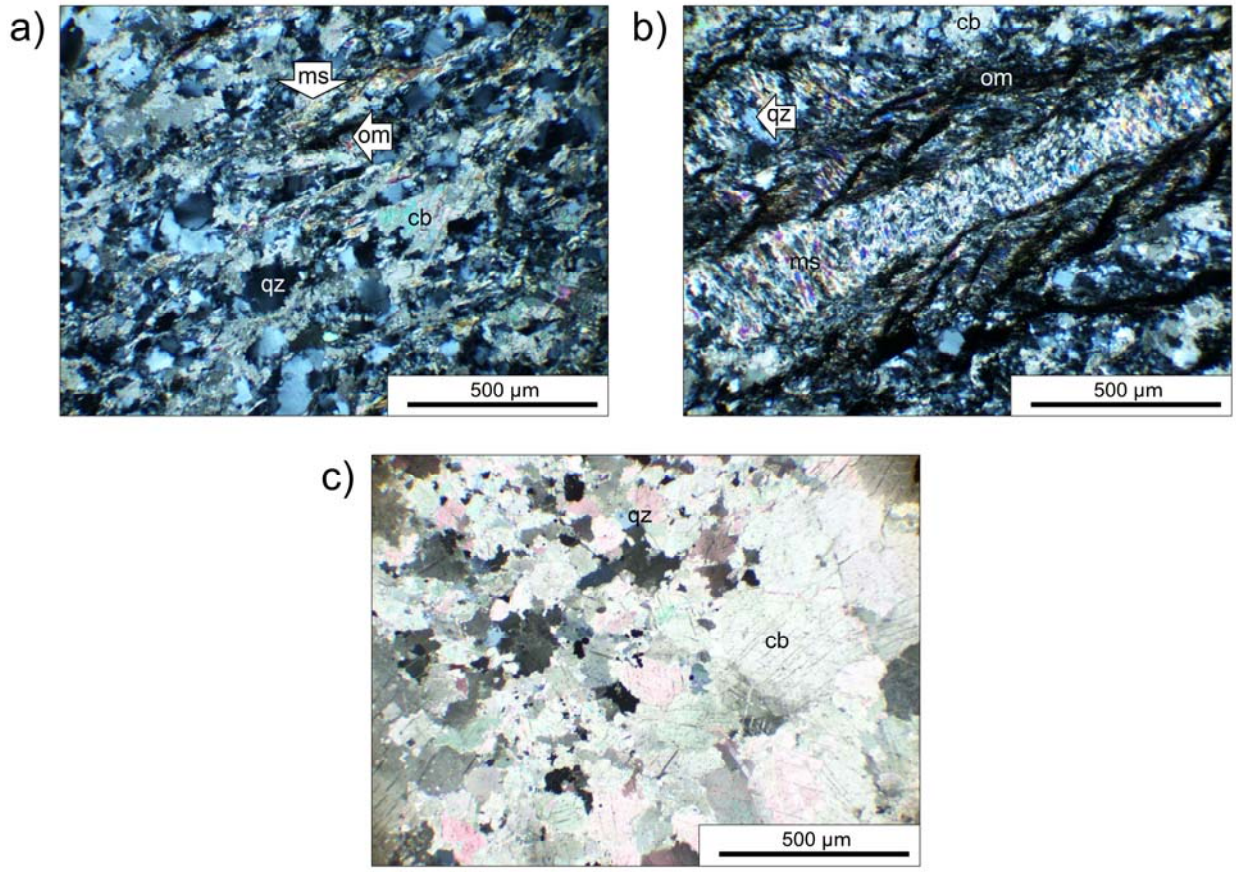

Fig. 2: Representative photomicrographs of host rocks: (a) Calcareous siltstones from interbedded calcareous siltstones-sandstones (104-01, 104D, depth 111.00 m). (b) Muscovite-organic matter bands intercalated by quartz-carbonate bands in interbedded carbonaceous shales and calcareous siltstones (104-12, 104D, depth 137.10 m). (c) Carbonate minerals and minor quartz in massive carbonate rocks (85-19, 085D, depth 103.50 m). The photomicrographs were taken under cross polarized light. Abbreviations: cb (carbonate minerals), ms (muscovite), om (organic matter), qz (quartz).

In contrast to the aforementioned units, the Jehe unit is composed of carbonate minerals. Quartz, muscovite and pyrite occur in minor amounts while zircon is present in trace amounts (Fig. 2c). Breccias and veins are common in the Jehe unit while quartz is present as the dominant cement and open-spaces filling mineral. The breccias and veins are a host to minor amounts of sphalerite and galena.

Geochemical data of the host rocks is presented in Table 1. The concentrations of S, Fe, Zn, Pb, Cu and As in the host rocks at the Anjing Hitam prospect are 0.01-3.52 wt%, 1.73-6.55 wt%, up to 4313 ppm, up to 12,395 ppm, up to 203 ppm and up to 221 ppm, respectively. The concentrations of Fe, Zn, Pb and As are moderately correlated to that of S as coefficients of correlation of these elements with respect to S in the Julu unit are 0.60, 0.33, 0.42 and 0.49, respectively. On the other hand, coefficient of correlation of concentrations of Cu and S is 0.04 suggesting that these elements are not correlated to

each other. Coefficients of correlation of Fe, Zn, Pb, Cu and As with respect to S in the Dagang and Jehe units were not determined since the number of data from these units is limited and these units do not host economically significant orebodies (Fig. 3).

Table 1: Geochemistry of host rocks.

Sample	Depth	S	Fe	Zn	Pb	Cu	As	Rock Unit
	(m)	wt%		ppm				
92-01	104.45	0.12	2.36	24	b.d.l.	12	4	Carbonaceous shales-calcareous siltstones
92-02	117.65	0.98	3.65	71	57	42	b.d.l.	Carbonaceous shales-calcareous siltstones
92-03	144.10	0.01	4.77	77	b.d.l.	b.d.l.	29	Carbonaceous shales-calcareous siltstones
92-07	159.70	1.48	2.44	82	1568	13	b.d.l.	Carbonaceous shales-calcareous siltstones
92-08	171.40	1.91	4.01	b.d.l.	b.d.l.	14	197	Carbonaceous shales-calcareous siltstones
29-18	155.70	0.26	2.28	147	17	22	b.d.l.	Calcareous siltstones-sandstones
29-19	165.50	0.70	2.41	b.d.l.	37	b.d.l.	18	Calcareous siltstones-sandstones
29-20	176.30	0.79	4.02	21	45	43	b.d.l.	Carbonaceous shales-calcareous siltstones
29-04	198.22	2.73	3.90	314	2081	b.d.l.	b.d.l.	Carbonaceous shales-calcareous siltstones
29-06	201.42	1.78	2.59	681	1324	5	b.d.l.	Carbonaceous shales-calcareous siltstones
29-07	203.42	1.77	3.90	3353	5962	15	b.d.l.	Carbonaceous shales-calcareous siltstones
29-09	215.81	0.47	2.86	b.d.l.	b.d.l.	59	8	Carbonaceous shales-calcareous siltstones
29-10	218.30	1.94	3.44	287	1459	41	b.d.l.	Carbonaceous shales-calcareous siltstones
29-11	220.75	1.19	2.51	b.d.l.	42	8	54	Carbonaceous shales-calcareous siltstones
29-14	237.00	0.65	3.00	70	413	13	b.d.l.	Carbonaceous shales-calcareous siltstones
29-16	255.52	1.71	3.19	32	252	32	221	Carbonaceous shales-calcareous siltstones
29-17	267.73	0.25	2.27	81	b.d.l.	b.d.l.	9	Massive carbonate rocks
104-01	111.00	0.45	1.92	b.d.l.	b.d.l.	6	177	Calcareous siltstones-sandstones
104-02	117.80	3.00	4.02	4313	2049	8	b.d.l.	Carbonaceous shales-calcareous siltstones
104-03	119.70	1.55	2.78	364	1020	b.d.l.	b.d.l.	Carbonaceous shales-calcareous siltstones
104-05	124.10	2.19	4.04	441	733	b.d.l.	9	Carbonaceous shales-calcareous siltstones
104-06	126.80	0.16	2.67	70	b.d.l.	30	b.d.l.	Carbonaceous shales-calcareous siltstones
104-09	130.85	1.10	2.36	b.d.l.	25	5	27	Carbonaceous shales-calcareous siltstones
104-10	132.20	0.61	3.45	b.d.l.	b.d.l.	74	5	Carbonaceous shales-calcareous siltstones
104-12	137.10	1.84	3.86	b.d.l.	b.d.l.	5	160	Carbonaceous shales-calcareous siltstones
104-16	165.70	0.13	2.70	21	b.d.l.	46	85	Carbonaceous shales-calcareous siltstones
104-17	171.50	0.06	3.72	22	b.d.l.	8	40	Carbonaceous shales-calcareous siltstones
104-18	185.10	0.10	1.92	294	72	b.d.l.	b.d.l.	Massive carbonate rocks
123-01	274.50	0.45	1.73	197	154	10	4	Carbonaceous shales-calcareous siltstones
123-02	294.85	0.42	3.49	b.d.l.	b.d.l.	22	b.d.l.	Carbonaceous shales-calcareous siltstones
123-03	315.80	0.09	4.67	b.d.l.	b.d.l.	16	50	Carbonaceous shales-calcareous siltstones
123-08	345.00	2.26	4.62	24	28	55	128	Carbonaceous shales-calcareous siltstones
85-06	34.80	0.81	3.43	361	70	32	41	Carbonaceous shales-calcareous siltstones
85-07	39.15	3.49	6.55	98	311	75	173	Carbonaceous shales-calcareous siltstones
85-08	47.80	0.54	2.95	37	19	42	17	Carbonaceous shales-calcareous siltstones
85-09	58.50	3.52	5.57	80	551	12	31	Carbonaceous shales-calcareous siltstones
85-12	72.95	3.19	5.52	b.d.l.	12395	15	b.d.l.	Carbonaceous shales-calcareous siltstones
85-13	76.00	1.16	2.46	1122	141	14	24	Carbonaceous shales-calcareous siltstones
85-14	81.65	1.49	4.75	b.d.l.	b.d.l.	203	46	Carbonaceous shales-calcareous siltstones
85-15	85.00	0.48	2.60	b.d.l.	b.d.l.	35	33	Carbonaceous shales-calcareous siltstones
85-16	91.44	0.25	2.17	b.d.l.	b.d.l.	8	61	Carbonaceous shales-calcareous siltstones
85-17	98.60	0.81	2.44	115	b.d.l.	b.d.l.	51	Carbonaceous shales-calcareous siltstones
85-19	103.50	0.35	2.18	b.d.l.	b.d.l.	6	16	Massive carbonate rocks

b.d.l.: below detection limit

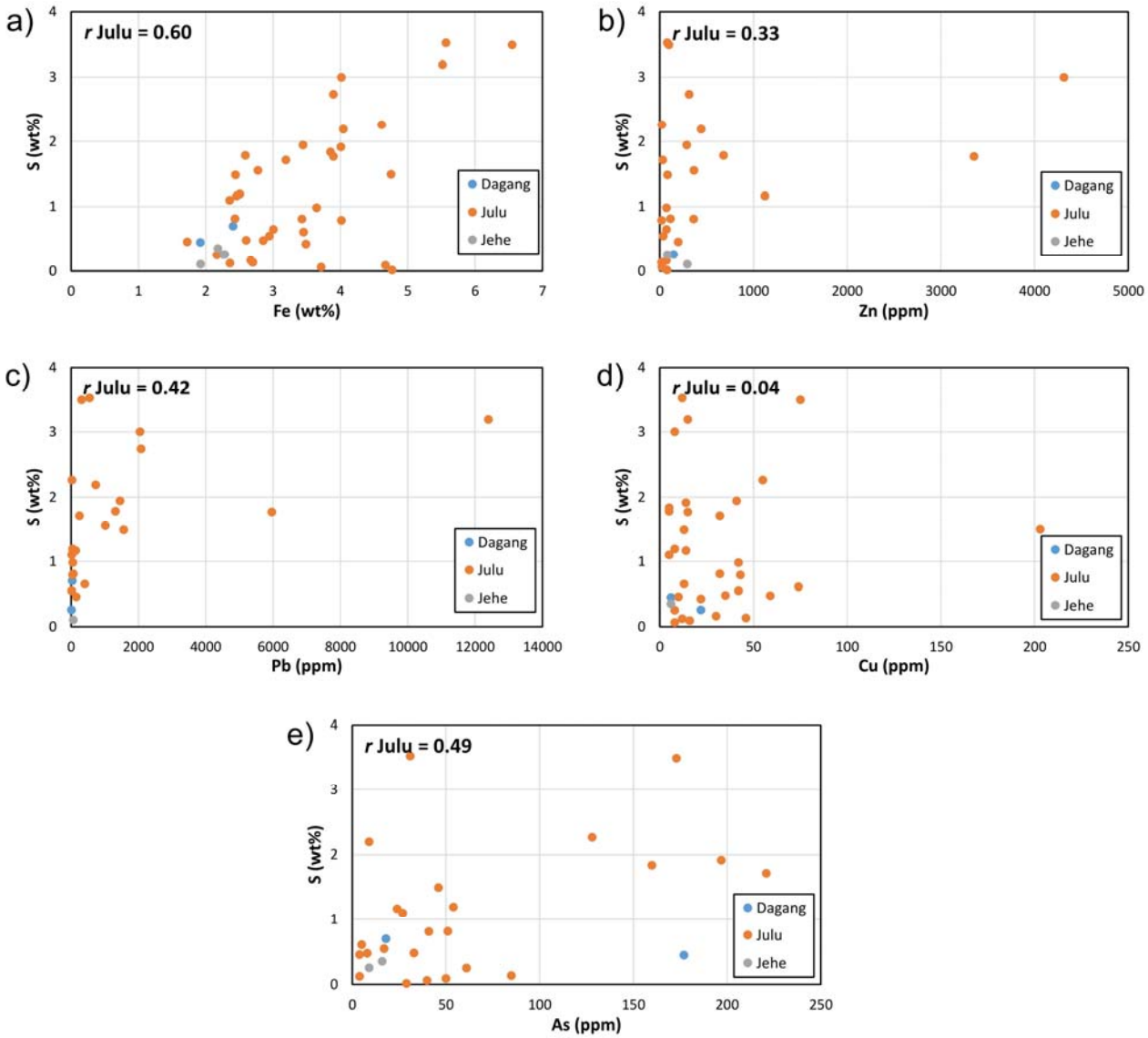

Fig. 3: Scatter plots illustrating the relationship between (a) Fe, (b) Zn, (c) Pb, (d) Cu, and (e) As vs S in host rocks.

4.2 Orebodies

According to ore minerals abundance and their textural relationship, the Anjing Hitam prospect hosts five ore types: (1) pyrite-rich massive ore, (2) sphalerite-rich massive ore, (3) bedded sulfide ore, (4) galena-rich breccia ore and (5) vein ore. Pyrite-rich massive ore is composed of abundant pyrite with sphalerite-galena intergrowth in the interstices (Fig. 4a). Sphalerite-rich massive ore is characterized by sphalerite-galena intergrowth with trace to minor amounts of pyrite (Fig. 4b). Bedded sulfide ore is identified as interbedded host rocks and sulfide-rich layers with individual layer up to 1 cm thick (Fig. 4c). The sulfide-rich layers are subdivided into pyrite-sphalerite-rich and galena-sphalerite-rich subtypes. Galena-rich breccia ore consists of host rock fragments cemented by galena with trace amounts of tetrahedrite, bournonite and pyrrhotite (Fig. 4d). Coarse-grained pyrite up to 3 mm in size also occurs in this ore type. Vein ore is associated with open-fracture filling in the host rocks and other ore types. This ore type is dominated by the sphalerite-galena intergrowth (Fig. 4e). Trace amounts of chalcopyrite locally occurs in all ore types as a disease in sphalerite.

Geochemical data of the orebodies is summarized in Table 2. Pyrite-rich massive ore contains S ranging from 21.27 to 24.39 wt%, Fe ranging from 14.63 to 19.76 wt%, Zn ranging from 5.44 to 13.55 wt%, Pb ranging from 1.99 to 21.32 wt%, Cu up to 29 ppm, Cd ranging from 220 to 688 ppm and As ranging from 875 to 10,718 ppm. Sphalerite-rich massive ore contains S ranging from 3.80 to 21.47 wt%, Fe ranging from 2.49 to 5.90 wt%, Zn ranging from 2.60 to 15.74 wt%, Pb ranging from 1.36 to 28.04 wt%, Cu up to 11 ppm, Cd ranging from 108 to 1864 ppm and As ranging from 438 to 13,702 ppm. Concentration of S in galena-rich breccia ore ranges from 1.30 to 8.56 wt% while those of Fe, Pb, Cu, Cd and As in this ore type range from 1.46 to 5.62 wt%, from 10.03 to 43.30 wt%, from 9 to 96 ppm, from 2 to 58 ppm and from

4,128 to 27,468 ppm, respectively. Zinc occurs in negligible amounts in galena-rich breccia ore. Concentrations of S, Fe, Zn, Pb, Cu, Cd and As in bedded sulfide and vein ores range within the interval ranges of these elements in the other ore types.

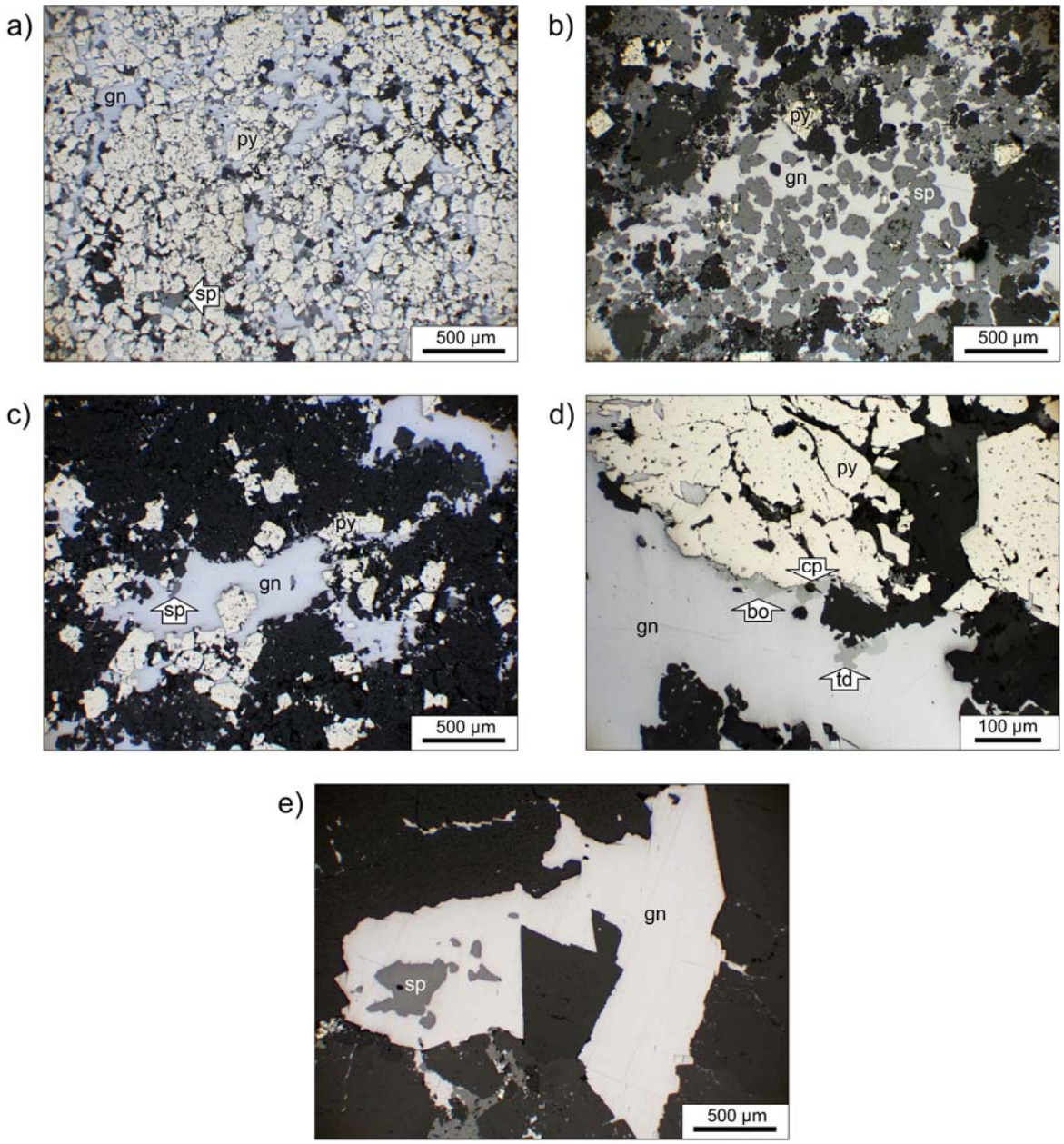

Fig. 4: Representative photomicrographs of orebodies: (a) Abundant cubic pyrite interstitially infilled by intergrowth of sphalerite and galena in pyrite-rich massive ore (104-04, 104D, depth 120.90 m). (b) Intergrowth of sphalerite and galena with minor cubic pyrite in sphalerite-rich massive ore (92-06, 092D, depth 154.15 m). (c) Galena-sphalerite-rich sulfide layer interbedded by host rock layers in bedded sulfide ore (104-07, 104D, depth 127.07 m). (d) The occurrence of bournonite and tetrahedrite in galena matrix surrounding exceptionally large, corroded, cubic pyrite in galena-rich breccia ore (92-04, 092D, depth 149.10 m). (e) Large, euhedral crystals of galena with sphalerite inclusions in vein ore. (29-02, 029D, depth 195.53 m). The photomicrographs were taken under parallel polarized light. Abbreviations: bournonite (bo), galena (gn), pyrite (po), sphalerite (sp), tetrahedrite (td).

Table 2: Geochemistry of orebodies.

Sample	Depth	S	Fe	Zn	Pb	Cu	Cd	As	Ore type
	(m)	wt%				ppm			
104-04	120.90	22.28	18.87	7.82	5.98	b.d.l.	288	2,601	Pyrite-rich massive ore
104-07	127.70	2.95	3.83	0.28	1.92	14	15	572	Bedded sulfide ore
104-11	134.20	23.30	18.46	11.49	9.49	b.d.l.	526	4,252	Pyrite-rich massive ore
104-13	142.44	23.42	17.67	13.55	8.51	2	688	3,634	Pyrite-rich massive ore
104-14	146.90	21.27	14.63	12.58	21.32	b.d.l.	581	10,718	Pyrite-rich massive ore
92-04	149.10	8.56	5.62	0.02	36.77	96	50	22,472	Galena-rich breccia ore
92-05	152.20	17.62	2.49	15.29	28.04	b.d.l.	1778	13,702	Sphalerite-rich massive ore
92-06	154.15	21.47	5.90	15.04	21.79	b.d.l.	1766	9,950	Sphalerite-rich massive ore
29-01	194.33	21.04	5.34	13.68	17.76	b.d.l.	1723	7,987	Sphalerite-rich massive ore
29-02	195.53	8.24	1.06	3.87	3.98	58	231	1,159	Vein ore
29-03	196.93	21.82	18.64	5.44	3.58	29	228	1,710	Pyrite-rich massive ore
29-08	207.65	22.16	18.56	9.78	5.54	28	220	2,415	Pyrite-rich massive ore
29-12	222.50	13.85	5.62	12.20	11.64	b.d.l.	888	4,938	Sphalerite-rich massive ore
29-15	242.00	6.12	2.28	0.01	43.30	15	58	27,468	Galena-rich breccia ore
123-04	320.40	15.35	4.26	13.30	18.91	b.d.l.	1139	8,870	Sphalerite-rich massive ore
123-05	327.43	20.82	4.27	15.74	27.46	b.d.l.	1864	13,326	Sphalerite-rich massive ore
123-06	334.60	19.97	5.58	13.67	17.22	b.d.l.	1551	7,594	Sphalerite-rich massive ore
85-03	20.30	8.64	2.74	11.77	12.88	b.d.l.	607	5,460	Sphalerite-rich massive ore
85-04	25.45	3.80	3.66	2.60	1.36	11	108	438	Sphalerite-rich massive ore
85-05	27.50	1.30	1.46	0.06	10.03	9	2	4,128	Galena-rich breccia ore
85-10	63.70	10.85	2.74	12.76	17.49	b.d.l.	761	8,091	Sphalerite-rich massive ore
85-11	68.60	24.39	19.76	9.93	1.99	5	416	875	Pyrite-rich massive ore

b.d.l.: below detection limit

The coefficients of correlation of Fe, Zn, Pb, Cd and As with respect to S in pyrite-rich massive ore are 0.62, 0.26, -0.53, 0.30 and -0.54, respectively. In sphalerite-rich massive ore, coefficients of correlation of these elements with respect to S are 0.57, 0.84, 0.78, 0.97 and 0.75, respectively. Coefficient of correlation of Cu vs S as well as those of other elements with respect to S in the other ore types were not determined since the number of data is limited (Fig. 5). In addition, coefficients of correlation were determined between Cd vs Zn and As vs Pb. The coefficients of correlation of Cd vs Zn in pyrite-rich massive ore and sphalerite-rich massive ore are 0.88 and 0.85, respectively, while those of As vs Pb in both ore types are 1.00 (Fig. 6).

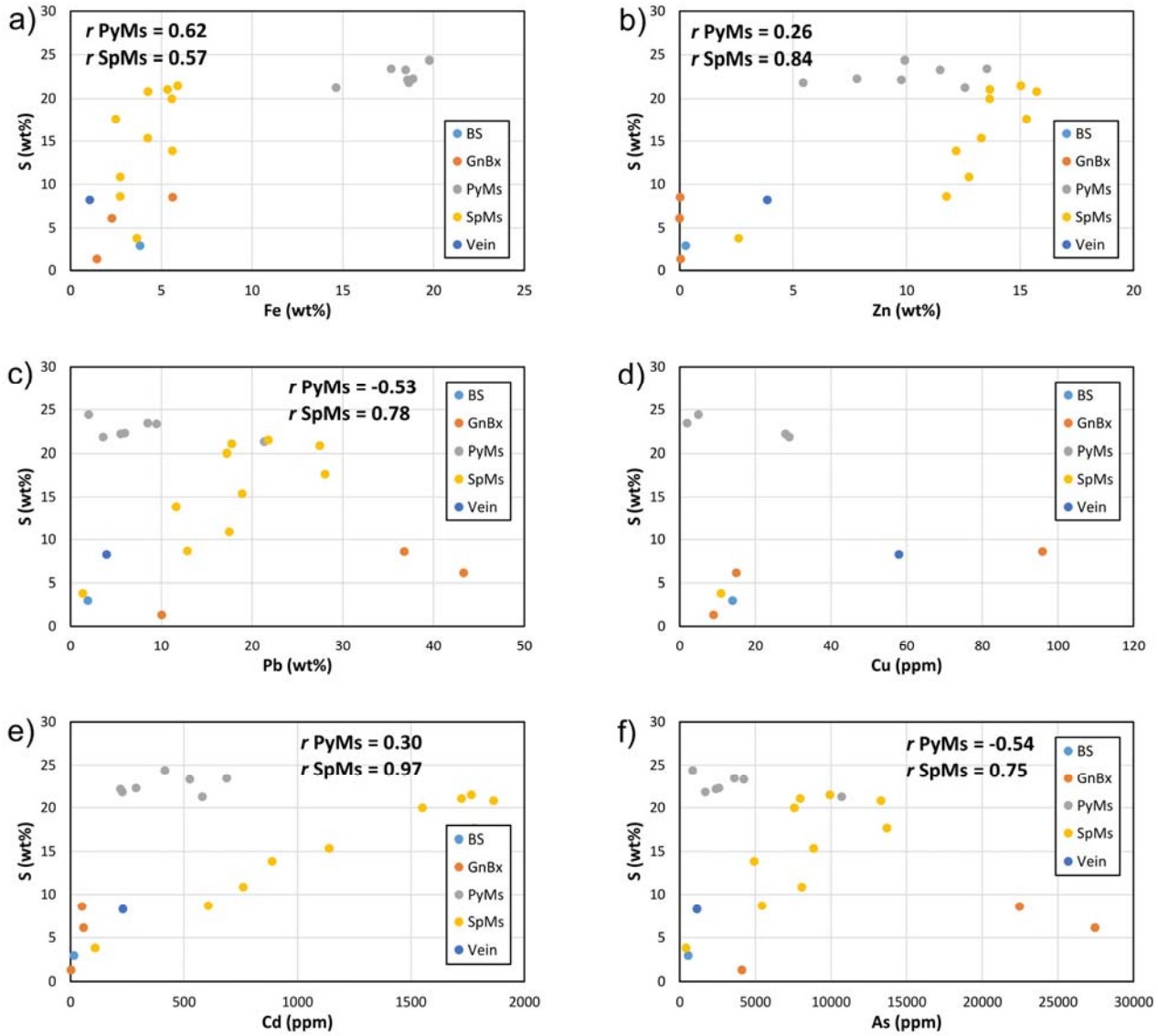

Fig. 5: Scatter plots illustrating the relationship between (a) Fe, (b) Zn, (c) Pb, (d) Cu, (e) Cd, and (f) As vs S in orebodies. Abbreviations: pyrite-rich massive ore (PyMs), sphalerite-rich massive ore (SpMs), bedded sulfide ore (BS), galena-rich breccia ore (GnBx).

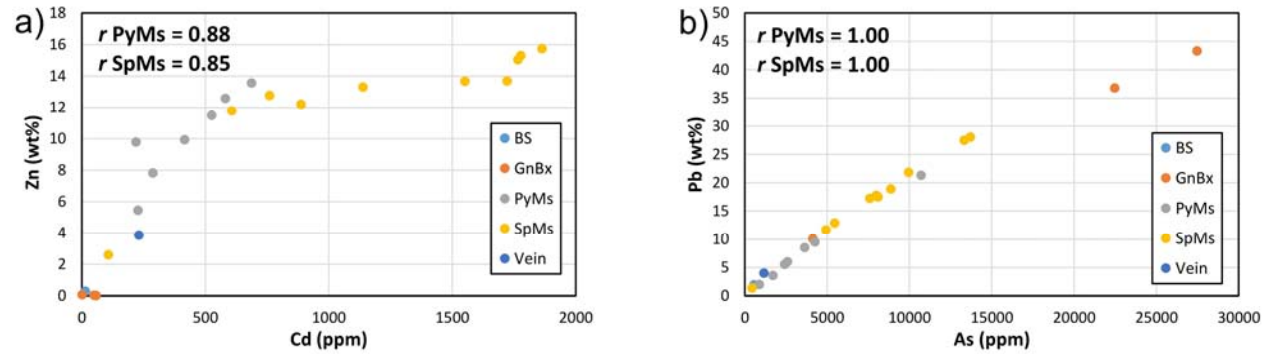

Fig. 6: Scatter plots illustrating the relationship between (a) Cd vs Zn and (b) As vs Pb in orebodies. Abbreviations: pyrite-rich massive ore (PyMs), sphalerite-rich massive ore (SpMs), bedded sulfide ore (BS), galena-rich breccia ore (GnBx).

5. Discussion

5.1 Mineralogy and Geochemistry

In the host rocks, the concentrations of Zn, Pb, Cu and As are generally in ppm level while those of S and Fe in wt% level. Locally, the concentrations of Zn and Pb are higher up to 4,313 and 12,395 ppm, respectively, occurring in the samples that display quartz-carbonate veins parallel to the sediment laminations. The locality of these samples corresponds to that of sphalerite and galena hosted in the lateral veins. The concentration of S is likely controlled by pyrite as the most common sulfide mineral in the Julu unit although the coefficient of correlation between Fe vs S shows that these elements are moderately correlated (r = 0.60). It is suggested that the moderate correlation between Fe and S is due to the presence of Fe in dolomite structure as this mineral composition shifts towards ankerite[17].

In the orebodies, the concentrations of S, Fe, Zn and Pb are generally in wt% level while those of Cu, Cd and As are in ppm level. The concentration of sulfur in the pyrite-rich massive ore is relatively centralized (21.3-24.4 wt%) and controlled by pyrite and sphalerite. Although galena is also present in pyrite-rich massive ore in significant amounts, its contribution to the concentration of sulfur is masked (r Pb vs S = -0.53) by a moderate control by pyrite (r Fe vs S = 0.62) and a weaker control by sphalerite (r Zn vs S = 0.26). In sphalerite-rich massive ore, the concentration of S is more dispersed than that of S in pyrite-rich massive ore. Sphalerite and galena in sphalerite-rich massive ore control the concentration of S in the ore type as indicated by strong correlation of S with Zn (r = 0.84) and Pb (r = 0.78). A moderate correlation between Fe and S in sphalerite-rich massive ore (r = 0.57) suggests that pyrite contribution to the concentration of S is not as significant as that of sphalerite and galena since pyrite occurs in a trace to minor amount.

Cadmium concentration in sphalerite-rich massive ore (607-1,864 ppm; excluding Cd concentration in sample 85-04) is higher than in the other ore types (2-688 ppm). The concentration of Cd is more strongly correlated to that of S in sphalerite-rich massive ore (r = 0.97) than in pyrite-rich massive ore (r = 0.30). Since independent CdS minerals (e.g. greenockite and hawleyite) are not present in the Anjing Hitam prospect, Cd should be present as an element in minerals that strongly control the concentration of S in sphalerite-rich massive ore and that can accommodate Cd in their structure, i.e. sphalerite. Similarities in chemical behaviors between Cd and Zn allow for replacement of Zn by Cd in Zn-bearing minerals[18]. The control of sphalerite over the concentration of Cd in this ore type is demonstrated by the coefficient of correlation between Cd and S (r = 0.85). The coefficient of correlation between Cd and S in the pyrite-rich massive ore (r = 0.88) also supports the idea that the presence of Cd in the Anjing Hitam prospect is controlled by sphalerite.

Arsenic has a strong correlation with S in sphalerite-rich massive ore (r = 0.75). Its correlation with S in pyrite-rich massive ore (r = -0.54) is poor, similar to that of Pb with S (r = -0.53). These correlations suggest that As is most likely controlled by galena. As mentioned above, galena is one of minerals controlling the concentration of S in sphalerite-rich massive ore and its contribution to the concentration of S in pyrite-rich massive ore is masked by other dominant sulfides, i.e. pyrite and sphalerite. The elevated concentrations of As in samples 92-04 (22,472 ppm) and 29-15 (27,468 ppm) were determined from galena-rich breccia ore which are dominated by galena. In this ore type, As-bearing minerals (tetrahedrite and bournonite) were observed as inclusions in galena.

5.2 Environmental Implications

5.2.1 Acid Mine Drainage

Mining exposes sulfide-rich rocks to the atmosphere that may come into contact with oxygen and water. The reaction between sulfide minerals, oxygen and water results in AMD. The resultant reaction of AMD generation with pyrite as an example is as follows:

$$2FeS_2(s) + 7.5O_2(g) = 2Fe(OH)_3(aq) + 4H_2SO_4(aq) + 7H_2O(l) \quad \text{... (1)}$$

The reaction above is accelerated by the presence of Thiobaccillus ferroxidans bacteria[19,20,21,22]. Although the principal economic sulfide minerals at the Anjing Hitam prospect (sphalerite and galena) will be recovered during ore processing, pyrite as a ubiquitous sulfide mineral will be dumped as tailings[2]. Pyrite-rich massive ore is a major ore type at the Anjing Hitam prospect and its S concentration is moderately controlled by the presence of pyrite. Pyrite as the controller of S concentration is also displayed in the host rocks. Pyrite is therefore a potential main contributor for the generation of AMD if it makes a contact with oxygen and water[18]. If the generation of AMD is not prevented, the released water from the mining sites is a potential pollutant agent for water bodies around the mining sites[23]. Furthermore, the increase in acidity of the released water leads to increase in metal mobility that may contaminate soils and ambient water[3].

5.2.2 Soil Acidification and Degradation

Soil acidification is an environmental issue that has been recognized due to mining and smelting activities[24]. Acid groundwater resulting from the interaction of groundwater and AMD is able to acidify soils around mining sites. Processing of metal sulfide minerals leads to the release of SO_2 gas from smelters which contributes to soil acidification[3]. Further impacts of soil acidification includes lowering soil fertility, diversity and population of soil biota and energy available for soil fauna[25,26,27]. In addition, acid soils are a favorable media in which metals are more mobile allowing easier metal uptake by plants[2]. As mentioned above, pyrite at the Anjing Hitam prospect dumped as tailings is a potential contributor in the

generation of AMD which can drive soil acidification. Sphalerite and galena processed in smelters generate SO_2 gas which is a responsible component in soil acidification.

5.2.3 Trace Element Contamination

Metals transported from the mining sites by AMD are a potential source of trace element contamination in the soils and water bodies. High acidity in the water released from the mining sites allow a higher solubility of metal in the water[2,3]. Metal oxides and sulfates accumulated in tailings are more soluble than their sulfide forms and are able to infiltrate deeper in the soils[2]. Besides being dispersed in water, contaminants are also able to disperse as solids and settle on the surface of plants. The dispersion of metals in the waters and as solids leads to trace element uptake by the plants, plant toxicity and the element transfer in the food chain[28,29,30,31]. Excessive trace element concentrations are toxic for plants, microbes, animals and humans[32].

Mining and smelting activities contribute to about 60% of Cd concentrations in the air[3]. In this study, the potential of Cd and Pb pollution is demonstrated as sphalerite (Cd-hosting mineral) and galena occur in abundant amounts at the Anjing Hitam prospect. Cadmium is a persistent element in nature and is easily absorbed by the plants. Likewise, Pb ore processing and smelting is the second most important source of anthropogenic Pb[3]. Association of Pb and As leads to the possibility of As contaminating the environment. Arsenic has been found as an uptake component by paddy rice[33] and other foods[34]. Therefore, trace element contamination is an important factor that has to be considered prior to the onset of mining and smelting activities at the Anjing Hitam prospect.

5.2.4 Human Health

Contamination by metals released from mining and smelting sites may endanger humans living around the mining sites. Lead and Cd can be transported as particulate matters and become a threat even long after mining and smelting activities cease[35,36,37,38]. Once mobile forms of Pb exist, contamination of drinking water may occur[39]. Neurological disorders and organ damage can occur even at low exposures of Pb and Cd[40]. Another threat is As contamination which can be transported in gaseous forms over a long distance. In the smelting processes of Zn-Pb ores, As is vaporized at temperature 615°C and released to the atmosphere[17]. Exposure to more than 100 ppm of As can cause death[41] and the worst mass poisoning in history was attributed to the use of As-bearing groundwater for drinking, cooking and irrigation[42].

Similar to trace element contamination, sphalerite and galena are two main minerals at the Anjing Hitam prospect that can endanger human health through Pb and Cd contamination if they are not properly treated. Galena also needs to be treated with care since it controls the concentration of As. Galena is a host to tetrahedrite and bournonite in galena-rich breccia ore. High concentration of As is also displayed by sphalerite-rich massive ore which contains a significant amount of galena.

6. Summary

Host rocks at the Anjing Hitam prospect are divided into Dagang (sandstones-siltstones), Julu (shales-siltstones) and Jehe (dolostones) units. Elevated concentrations of Zn and Pb were identified in the rocks displaying lateral quartz-carbonate veins in the footwall sequence relative to orebodies. Concentration of S in the host rocks is controlled by pyrite.

The orebodies display five ore types: pyrite-rich massive ore, sphalerite-rich massive ore, bedded sulfide ore, galena-rich breccia ore and vein ore. Pyrite controls concentration of S in pyrite-rich massive ore as does sphalerite in pyrite-rich and sphalerite-rich massive ore. Concentration of S in sphalerite-rich massive ore is also partially controlled by galena. Concentration of Cd is controlled by sphalerite while that of As is controlled by galena.

Several environmental implications at the Anjing Hitam prospect may occur due to mining and smelting activities in the future. The potential environmental issues include acid mine drainage, soil acidification and degradation, trace element contamination and human health problems.

Acknowledgements

Many thanks are addressed to management and staffs of PT Bumi Resources Minerals, Tbk. for supporting our fieldworks and supplying secondary data. Financial support of this study is partially provided by Advanced Graduate Program in Global Strategy for Green Asia, Kyushu University. We also would like to thank Jacob Kaavera and Albano Mahecha for their significant insights and invaluable discussion.

References

1) A. Aykol, M. Budakoglu, M. Kumral, A.H. Gultekin, M. Turhan, V. Esenli, F. Yavuz and Y. Orgun, *Environ. Geol.*, **45**, 198-208 (2003).
2) D.L. Sorensen, W.A. Kneib, D.B. Porcella and B.Z. Richardson, *J. Environ. Qual.*, **3**, 162-166 (1980).
3) S. Dudka and D.C. Adriano, *J. Environ. Qual.*, **26**, 590-602 (1997).
4) G. Merrington and B.J. Alloway, *Appl. Geochem.*, **9**, p. 677-687 (1994).
5) J. Routh and M. Ikramuddin, *Chem. Geol.*, **133**, 221-224 (1996).
6) U. Rösner, *Environ. Geol.*, **33**, 224-230 (1998).
7) M.B. Parsons, D.K. Bird, M.T. Einaudi and C.N. Alpers, *Appl. Geochem.*, **16**, 1567-1593 (2001).
8) M. Benvenuti, I. Mascaro, F. Corsini, P. Lattanzi, P.

Parrini and G. Tanelli, *Environ. Geol.*, **30**, 238-243 (1995).
9) D. Banks, P.L. Younger, R.T. Arnesen, E.R. Iversen and S.B. Banks, *Environ. Geol.*, **32**, 238-243 (1997).
10) M.P. Boulet and A.C.L. Larocque, *Environ. Geol.*, **33**, 130-142 (1998).
11) B.G. Lottermoser, P.M. Ashley and D.C. Lawiem *Environ. Geol.*, **39**, 61-74 (1999).
12) C.H. Lee, H.K. Lee and J.C. Lee, *Environ. Geol.*, **40**, 482-494 (2000).
13) M.J. Marques, E. Martinez-Conde and J.V. Rovira, *Environ. Geol.*, **40**, 1125-1137 (2001).
14) S. Dwiki, *Evergreen*, **5**, 50-57 (2018).
15) T.A. Rivai, K. Yonezu, K. Watanabe, Syafrizal, A.J. Boyce and K. Sanematsu, in *the Society of Resource Geology Abstract with Programs 68*, the Society of Resource Geology (2018).
16) T.W. Middleton, The Dairi zinc-lead project, North Sumatra, Indonesia – discovery to feasibility study. http://www.smedg.org.au accessed February 15, 2019 (2003).
17) P.E. Rosenberg and F.F. Foit Jr., *Geochim. Cosmochim. Ac.*, **43**, 951-955 (1979).
18) M. Gutiérrez, K. Mickus and LM. Camacho, *Sci. Total Environ.*, **565**, 392-400 (2016).
19) D.K. Nordstorm, in *Acid sulfate weathering*, eds. by J.A. Kittrick, D.S. Fanning and L.R. Hosner, SSSA Special Publication 10, SSSA, Madison, Wisconsin (1982).
20) A. Akcil and S. Koldas, *J. Clean. Prod.*, **14**, 1139-1145 (2006).
21) D.B. Johnson and K.B. Hallberg, *Sci. Total Environ.*, 3-14 (2005).
22) B.J. Baker and J.F. Banfield, *Microb. Ecol.*, **44**, 139-152 (2003).
23) A. Peppas, K. Komnitsas and I. Halikia, *Miner. Eng.*, **13**, 563-574.
24) S.S. Dixit, A.S. Dixit and J.P. Smol, *Can. J. Fish. Aquat. Sci.*, **49**, 8-16 (1992).
25) M.H. Donker, *Func. Ecol.*, **6**, 445-454 (1992).
26) C.D. Maxwell, *Water, Air, and Soil Pollution*, **60**, 381-393 (1991).
27) C.D. Maxwell, in *Environmental restoration of the industrial city*, eds. by R. Lal and B.A. Stewart, Springer-Verlag, Berlin, p. 219-231 (1995).
28) S. Dudka, R. Ponce-Hernandez, G. Tate and T.C. Hutchinson, *Water, Air, and Soil Pollution*, **90**, 531-542 (1996).
29) K. Winterhalder, *Environ. Rev.*, **4**, 185-224 (1996).
30) R.L. Chaney, W.N. Beyer, C.H. Gifford and L. Sileo, in *Trace substances in environmental health-22*, ed. by D.D. Hemphill, Univ. of Missouri, Columbia, p. 263-280 (1988).
31) F. Rebele, A. Surma, C. Kuznik, R. Bornkamm and T. Brej, *Acta Soc. Bot. Pol.*, **62**, 53-57 (1993).
32) D.L. Sparks, *Elements*, **1**, 193-197 (2005).
33) P.N. Williams, A.H. Price, A. Raab, S.A. Hossain, J. Feldmann and A.A. Mehard, *Environ. Sci. Tech.*, **39**, 5531-5540 (2005).
34) S.W. Al Rmalli, P.I. Haris, C.F. Harrington and M. Ayub, *Sci. Total Environ.*, **337**, 23-30 (2005).
35) D.C. Adriano, *Trace elements in the terrestrial environment*, 2nd ed, Springer-Verlag, New York (2001).
36) D.C. Adriano, N.S. Bolan, J. Vangronsveld and W.W. Winzel, in *Encyclopedia of soils in the environment*, ed. by D. Hillel, Elsevier, Amsterdam, p. 175-182 (2005).
37) C. Lei, B. Yan, T. Chen, S.X. Quan and X.M. Xiao, *J. Environ. Chem. Eng.*, **3**, 862-869.
38) H.Y. Zhan, Y.F. Jiang, J. Yuan, X.F. Hu, O.N. Nartey and B.L. Wang, *J. Geochem. Explor.*, **149**, 182-188 (2014).
39) World Health Organization (WHO), Lead poisoning and health. Fact Sheet 379 Reviewed August 2015 www.who.int/mediacentre/factsheets/fs379/en/ accessed November 5, 2018 (2015).
40) P.B. Tchounwou, C.G. Yedjou, A.K. Patlolla and D.J. Sutton, in *Molecular clinical environmental toxicology volume 3: environmental toxicology*, ed. by A. Luch, Springer Nature, Switzerland, p. 133-164 (2012).
41) A. Leonard, in *Metals and their compounds in the environment*, ed. by E. Merian, VCH, New York, p. 751-774 (1991).
42) A.H. Smith, E.O. Lingas and M. Rahman, *B. World Health Organ.*, **78**, 1093-1103 (2000).